Bayesian Statistics to Elucidate the Kinetics of γ-Valerolactone from n -Butyl Levulinate Hydrogenation over Ru/C

Sarah Capecci, Yanjun Wang, Jose Delgado, Valeria Casson Moreno, Mélanie Mignot, Henrik Grénman, Dmitry Yu. Murzin, Sébastien Leveneur

Bayesian statistics to elucidate the kinetics of γ-valerolactone from n-butyl levulinate hydrogenation over Ru/C

Sarah Capecci[1,2†], Yanjun Wang[1†], Jose Delgado[1,4], Valeria Casson Moreno[2], Mélanie Mignot[3], Henrik Grénman[4], Dmitry Yu. Murzin[4], Sébastien Leveneur[1*]

[1]*Normandie Univ, INSA Rouen, UNIROUEN, LSPC, EA4704, 76000 Rouen, France*

[2]*Dipartimento di Ingegneria Chimica, Civile, Ambientale e dei Materiali, Alma Mater Studiorum—Università di Bologna, via Terracini 28, 40131 Bologna, Italy*

[3]*COBRA UMR CNRS 6014, Normandie Université, INSA de Rouen, avenue de l'Université, Saint-Etienne-du-Rouvray, 76800, France*

[4]*Laboratory of Industrial Chemistry & Reaction Engineering, Department of Chemical Engineering, Johan Gadolin Process Chemistry Centre, Åbo Akademi University, FI-20500 Åbo-Turku, Finland*

**sebastien.leveneur@insa-rouen.fr*

† These authors contributed equally to the work.

Abstract

Synthesis of γ-valerolactone (GVL), a platform molecule that can be produced from lignocellulosic biomass, was performed in this work by hydrogenation of an alkyl levulinate over Ru/C. Kinetic models reported in the literature are typically not compared with rival alternatives, even if a discrimination study is needed to find the optimum operating conditions. Different surface reaction kinetic models were thus considered in this work, specifically addressing hydrogenation of butyl levulinate to GVL, where the latter was used as a solvent to minimize potential solvent interference with the reaction, including its evaporation. The Bayesian approach was applied to evaluate the probability of each model. It was found that non-competitive Langmuir-Hinshelwood with no dissociation of hydrogen model has the highest posterior probability.

Keywords: Bayesian statistics, γ-valerolactone, model discrimination, kinetic modeling, hydrogenation.

1. INTRODUCTION

Over the past few decades, the need for climate change mitigation and management of a potential energy crisis has led to the exploitation of biomass to produce biofuels, biochemicals and biomaterials [1]. In particular, the use of non-edible lignocellulosic biomass (e.g. agricultural residues, energy crops, forestry, and industrial wastes) can be seen as a strategy to enhance the cleaner production of renewable fuels, chemicals and materials and to fulfill the demands of a growing population [2], avoiding the competition with food crops and having a significant impact on the worldwide rural economy.

A pre-treatment process of the lignocellulosic biomass (for example, biological, thermochemical, catalytic or a combination of them) allows besides an easy removal of so-called extractives, also the production of different organic compounds, such as sugars, polyols, furanics, as well as several acids (e.g., levulinic acid, succinic acid, 3-hydroxy-propionic acid, etc.). These compounds can be used as starting materials (so-called platform molecules) to synthesize numerous value-added chemicals, fuel additives, solvents and paintings, novel monomers, etc. [3]. Among all possible platform molecules that can be derived from lignocellulosic biomass refinery, levulinic acid (LA) is considered as one of the top value-added chemicals, being the basis for the synthesis of other important chemicals, such as γ-valerolactone (GVL) [4].

GVL is a major precursor in biorefinery. It is characterized by interesting physical-chemical properties, being stable in water (no hydrolysis under neutral conditions) and in the presence of air (minimal if any formation of peroxides), making it a safe material for various industrial applications [5]. Other significant features of GVL are related to its fuel properties that are comparable to ethanol. In summary, GVL is renewable, stable and non-toxic [6]. It can be used as a precursor of gasoline and diesel fuels, as a green solvent in fine chemical synthesis and food additives, and as an

intermediate in the synthesis of many value-added chemicals (e.g., adipic acid, the precursor of nylon) [2].

The most common method for the production of GVL is the hydrogenation of LA or alkyl levulinates. One can distinguish different methods[5,7,8] such as the use of molecular hydrogen[9–19]; in-situ decomposition of formic acid to hydrogen[10,14,20–29]; alcohols for catalytic transfer hydrogenation by the Meerwein-Ponndorf-Verley reaction[30–31,32] or via the catalytic hydrogenation of 4-hydroxyvaleric acid [4].

On the one hand, because of the easy access to the active catalytic center, in the last 20 years, many homogeneous catalysts have been developed to hydrogenate LA to GVL; among all, Ru-based catalysts are the most attractive and have been widely studied [5]. On the other hand, homogeneous systems are challenging when it comes to product separation because of GVL high boiling point (207–208 °C) distillation is not economically attractive [6]. In recent years, this problem was partially overcome by confining the catalysts within a not-aqueous phase, enabling product separation and catalyst recycling. Nevertheless, such an approach is limited to a single catalyst recycle only and leads to a considerable decrease in LA conversion (81 vs. 55 %) [6]. To favor downstream processes, a cost-efficient GVL large-scale production should be more oriented toward heterogeneous catalysis.

Despite several attempts to develop vapor-phase hydrogenation continuous processes to produce GVL from LA, which were proved to be not favorable in terms of selectivity and energy demand [6], most of the studies are focusing on the liquid-phase hydrogenation systems aimed at the direct conversion of aqueous LA to GVL. The simplest and oldest systems involved transition metals as a catalyst; more recently and actually, supported metal catalysts have been and are extensively investigated. Among all, Ru/C resulted in being the most active, leading to the highest conversion

(> 95 %) and selectivity (≈ 99%) [6]. The optimal operating temperature was found to be 130°C, with higher reaction temperatures causing a decrease in GVL yields. Another critical parameter influencing the GVL yield in heterogeneous catalysts is the support nature [33].

The current work focuses on the heterogeneous catalytic hydrogenation of butyl levulinate (BL) to GVL over a catalyst with non-acidic support, namely Ru/C.

The BL hydrogenation process to produce GVL is based on a two-step reaction, as depicted in Figure 1[34]. In the first step, the Ru/C catalyzed hydrogenation of butyl levulinate takes place, leading to an intermediate formation. In the case of BL hydrogenation, the intermediate is butyl 4-hydroxypentanoate (BHP). In the second step, the intra-cyclization of the intermediate occurs to form GVL.

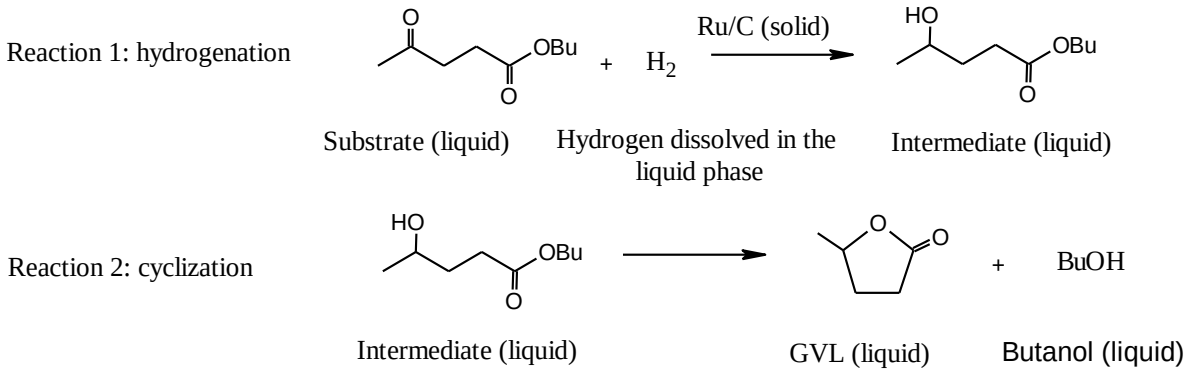

Figure 1. Reaction scheme of hydrogenation of butyl levulinate to GVL.

Piskun et al. [35] showed that for the hydrogenation of levulinic acid in a water solvent, protons (Brønsted acid) from levulinic acid dissociation could catalyze the second step. The second step can also be catalyzed by the presence of Lewis sites on the catalyst that could enhance the rate of the ring closure, as recently demonstrated by Li et al. [36]. The positive influence of the Lewis sites on the selective formation of GVL was also reported in the study of Kasar et al. [37], reporting hydrogenation of LA catalyzed by bimetallic Ru−Ni/MMT, where an alternative to Figure 1 path

was realized, namely, α-angelica lactone was found to be the intermediate undergoing hydrogenation by dissociatively adsorbed hydrogen to form GVL.

As previously mentioned, the hydrogenation of LA was widely explored in the last years, and, in the literature, one can find several models for its hydrogenation to produce GVL with different catalysts, different support materials and solvents [34,35,38–41].

Although several esters of levulinic acid were applied in the literature, the choice of butyl levulinate as the substrate and GVL as the solvent in this study was motivated by its high vapor pressures limiting evaporation [42]. Furthermore, it was shown that the thermal risk was lower for the hydrogenation of BL over Ru/C compared to the hydrogenation of methyl levulinate over Ru/C [43]. Indeed, the kinetics of BL hydrogenation was shown to be slower than that for methyl levulinate, and the reaction enthalpy of BL hydrogenation was found to be lower than the corresponding value for methyl levulinate. Besides, the production of BL from the alcoholysis of carbohydrates is a promising route [44,45], justifying the utilization of BL as a reactant in the current work. Also, levulinic acid induces corrosive issues at high temperature [46,47].

More specifically, this study aimed to elucidate the reaction kinetics considering different reaction mechanisms applying the Bayesian statistical approaches described in the literature [48]. Bayesian approach is an excellent decision tool to select the most probable model via the calculation of the posterior density[49].

2. MATERIALS AND METHODS

2.1 Chemicals

For the experiments and the analytical part, different chemicals were used without further purification: γ-valerolactone (wt% ⩾ 99%) from Sigma Aldrich; Ru/C catalyst (Ruthenium, 5% on activated carbon powder, standard, reduced, nominally 50% water wet), n-butyl levulinate (wt% ⩾ 98%) and butanol (wt% ⩾ 98%) were purchased from Alfa Aesar; hydrogen gas (H_2 purity > 99,999 vol%) was from Linde; acetone (analytical grade) and furfural were from VWR from Acros Organics, respectively.

2.2 Analytical methods

The concentrations of n-butyl levulinate and intermediate products were measured by GC-FID. The GC-FID apparatus is a Bruker Scion GC436 equipped with a flame ionization detector, an autosampler and a capillary column (Rxi-5 ms, 30 m x 0.32 mm internal diameter x 0.25 μm film thickness). The carrier gas was Helium (99.99%), and it was used at a constant flow rate of 1.2 $mL.min^{-1}$. A temperature of 270°C was used for the injector and the detector. The oven temperature was set according to the following program 35°C (3 min) - 15°C min^{-1} - 300°C. The total run time was 21 min. The injection volume was 0.2 μL, and the split ratio is 30:1. Furfural was used as an internal standard. The concentration measurement uncertainty was evaluated via the standard deviation of replicate measurements. The standard deviations for BL and the intermediates concentrations were found to be lower than 1% and 0.8%, respectively.

2.3 Kinetic experiments

The kinetic experiments were conducted under isothermal and isobaric conditions in a 300 mL stainless steel Parr reactor operating in a batch mode (Figure 2). Efficient agitation was ensured by a gas entrainment impeller comprising a hollow shaft.

The hydrogen was provided through a 0.5 L reservoir connected to a gas bottle. The uncertainty for pressure transducers was 0.1 bar, and 0.1°C for temperature probes.

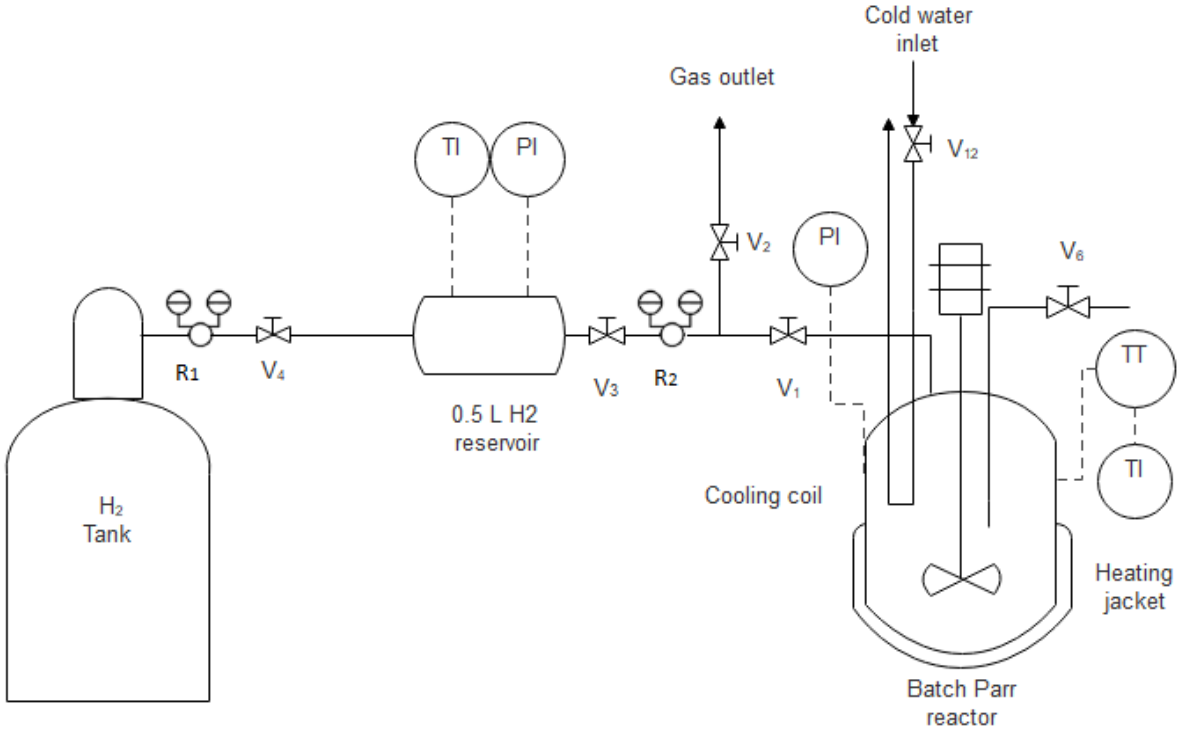

Figure 2. Experimental scheme of the reactor setup.

In the first step, the desired amount of reactants, the solvent and the catalyst (untreated) were loaded into the reactor. The reactor was sealed, and the air was removed by a vacuum pump. In order to homogenize the mixture temperature, the agitation velocity was set at 400 rpm. Once the desired temperature was reached, the valve V1 was opened, allowing hydrogen to flow to the reactor. The agitation rate was set at 1000 rpm, which based on a previous study, was found to be sufficient for

overcoming gas-liquid and liquid-solid external mass transfers [34]. Wang et al. [34] also showed that internal mass transfer can also be neglected.

During a kinetic experiment, several samples were withdrawn periodically from the reactor through valve V6. These samples were filtered to separate the reaction mixture and the catalyst. For the success of the parameter estimation stage, it is fundamental to vary the operating conditions (reaction temperature, hydrogen pressure, catalyst loading, concentrations, etc.). These variations are shown in Table 1, which is the experimental matrix.

Table 1. Experimental matrix for the kinetic study.

Exp.	H_2 press. bar	Temp K	m_{cat} kg (50%wt moisture)	$[BL]_0$ mol/m^3	$[Interm]_0$ mol/m^3	$[GVL]_0$ mol/m^3	$[BuOH]_0$ mol/m^3
1	23.4	403.15	0.0028	1834	0	6833	0
2	23.3	413.15	0.0028	866	0	8831	0
3	22.3	423.15	0.0018	807	0	8515	0
4	22.3	407.15	0.0028	839	0	8877	0
5	22.3	427.15	0.0028	619	0	8827	0
6	20.0	403.15	0.0028	868	0	8755	0
7	23.8	373.20	0.0005	1821	0	6851	0
8	23.3	423.15	0.0000	59	1586	6884	189
9	16.3	373.15	0.0005	1893	0	6719	0
10	11.4	373.15	0.0005	1821	0	6675	0
11	5.2	393.15	0.0010	1885	0	6720	0
12	23.7	413.15	0.0000	56	1411	7120	168

3. RESULTS AND DISCUSSION

3.1 Influence of reaction parameters and deactivation

As found in a previous article of our group [34], under the experimental conditions applied in this manuscript, there are no external or internal mass transfer limitations. To compare the effects of initial reaction parameters on the kinetics, the following normalized values were used: $\frac{[BL]}{[BL]_0}$ and $\frac{[BHP]}{[BL]_0}$.

3.1.1 Effect of hydrogen pressure

To evaluate the effect of hydrogen pressure on the kinetics, Experiments 7, 9 and 10 (Table 1) were compared. Figures 3A-B display the evolution of $\frac{[BL]}{[BL]_0}$ and $\frac{[BHP]}{[BL]_0}$ versus reaction time. As can be seen at lower pressures, there is a minor effect of hydrogen pressure on the kinetics of BL hydrogenation, which becomes negligible upon pressure elevation (Figure 3.A). Figure 3.B shows that the conversion of BHP to GVL is the slowest step.

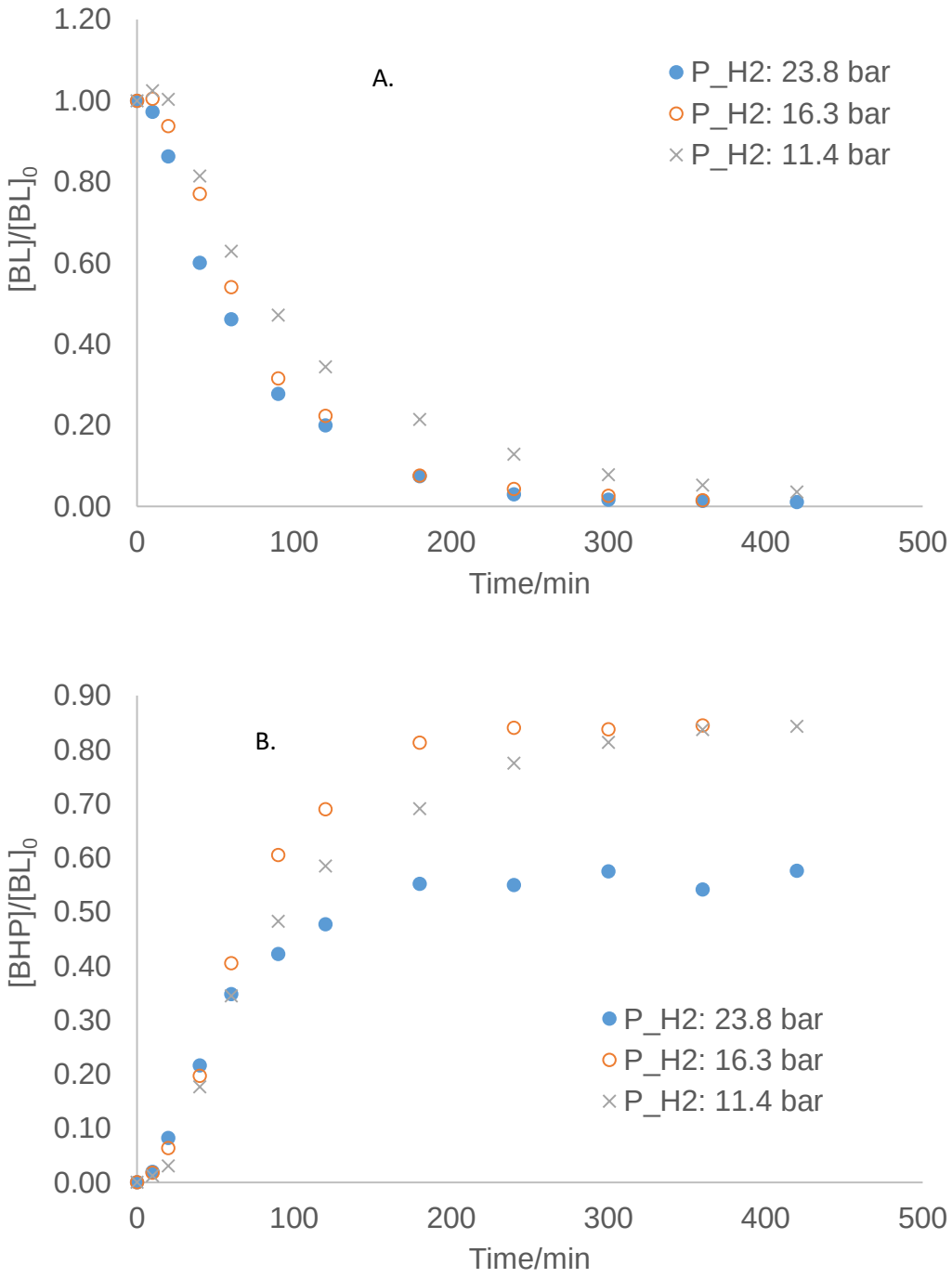

Figure 3. Effect of pressure on A) $\frac{[BL]}{[BL]_0}$ and B) $\frac{[BHP]}{[BL]_0}$ at 100°C (Experiments 7; 9 & 10).

3.1.2 Effect of reaction temperature

To evaluate the effect of reaction temperature on the kinetics, Experiments 2, 5 and 6 were compared. Figures 4A-B display the evolution of $\frac{[BL]}{[BL]_0}$ and $\frac{[BHP]}{[BL]_0}$ versus reaction time at different temperatures, it is clearly illustrating a positive effect of the temperature elevation. A detailed analysis of the activation energies will be presented below.

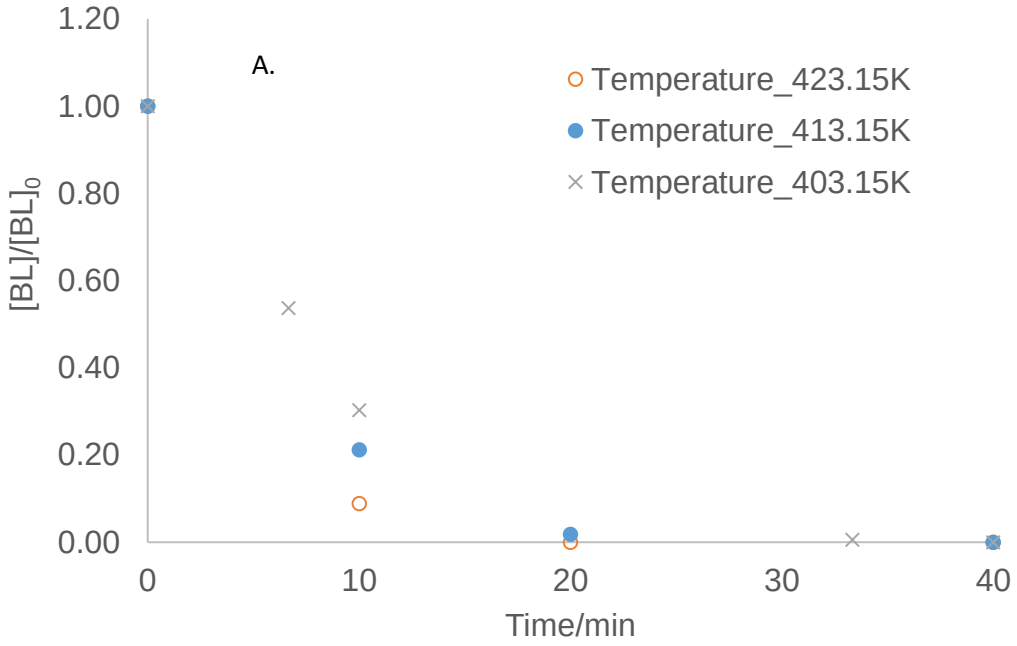

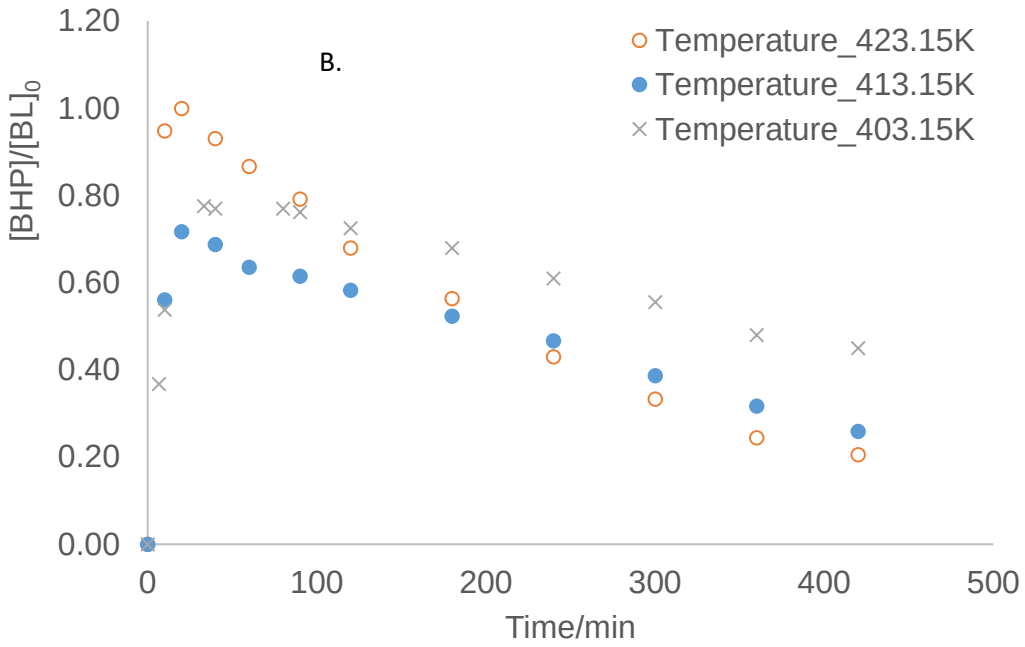

Figure 4. Effect of temperature on A) $\frac{[BL]}{[BL]_0}$ and B) $\frac{[BHP]}{[BL]_0}$ at 20 bars (Experiments 2, 5 & 6).

3.1.3 Effect of the catalyst amount

To evaluate the effect of the catalyst amount on the kinetics, Experiments 3 and 5 were compared. Figures 5A-B display the evolution of $\frac{[BL]}{[BL]_0}$ and $\frac{[BHP]}{[BL]_0}$ versus reaction time. The increase of catalyst amount increases the kinetics of the conversions of BL to BHP. As the first step is fast, the kinetics of conversion of BHP to GVL also increases.

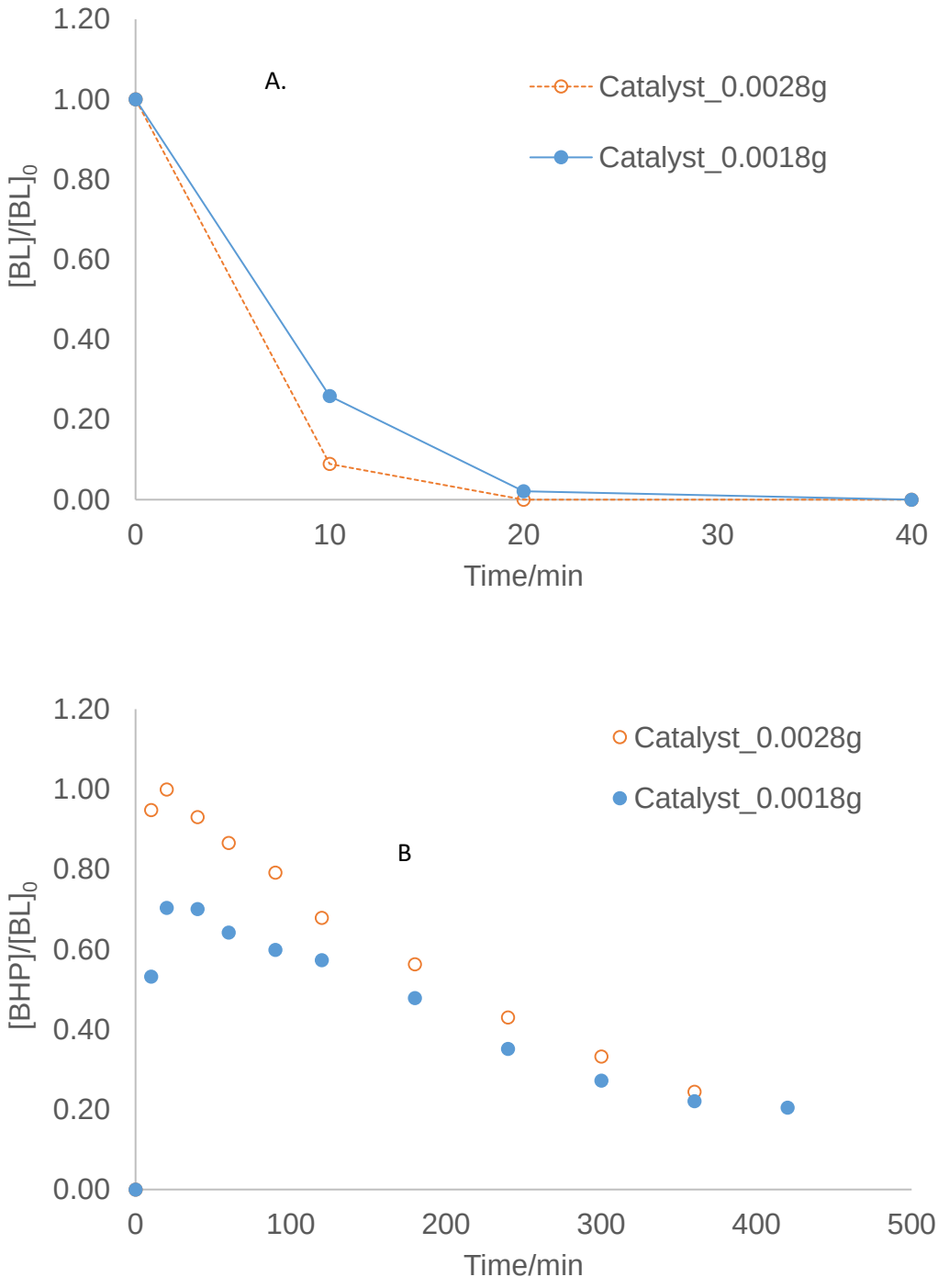

Figure 5. Effect of catalyst amount on A) $\frac{[BL]}{[BL]_0}$ and B) $\frac{[BHP]}{[BL]_0}$ at 20 bars and 150°C (Experiments 3 & 5).

3.2 Kinetic modeling

3.2.1 Kinetics

From the experimental results and the literature data, hydrogenation of BL to GVL over Ru/C is a two-step reaction (Figure 1). The first step is the hydrogenation of the carbonyl group, leading to the intermediate butyl 4-hydroxypentanoate (BHP). The second step is the cyclization of this intermediate, leading to the production of butanol and GVL.

In the kinetic analysis of the reaction performed by Wang et al. [34], power-law rate expressions were used for both stages. In the current work, mechanistic expressions were employed considering, for example, that the first step can proceed by several mechanisms, including competitive or non-competitive Langmuir-Hinshelwood ones with molecular or dissociative hydrogen adsorption in both cases as well as the Eley-Rideal mechanism without any adsorption of hydrogen.

For the second reaction, i.e., cyclization, both non-catalytic and catalytic pathways are possible. The latter pathway was introduced considering that the carbon supports exhibit typically low but not negligible acidity.

Overall, ten kinetic models can be derived, as summarized in Table 2, with the details of derivations available in Supporting Information. In the kinetic expressions, adsorption of GVL was considered to be negligible, otherwise hindering significantly the rate of BL hydrogenation, which proceeds relatively fast in GVL as a solvent.

Table 2. Rate expressions of the hydrogenation step.

MODELS	Rate expression
Langmuir Hinshelwood with molecular adsorption of H_2 (LH1)	$\frac{k_1 * K_{H2} * [H_2] * K_{BL} * [BL] * \omega_{Cat.}}{(K_{H2} * [H_2] + K_{BL} * [BL] + K_{BHP} * [BHP] + 1)^2}$
Langmuir Hinshelwood with hydrogen dissociation (LH2)	$\frac{k_1 * K_H * [H_2] * K_i * K_{BL} * [BL] * \omega_{Cat.}}{\left(\sqrt{K_H * [H_2]} + K_{BL} * [BL] + K_{BHP} * [BHP] + K_i * K_{BL} * [BL] * \sqrt{K_H * [H_2]} + 1\right)^2}$
Eley-Rideal with no adsorption of hydrogen (ER1)	$\frac{k_1 * [H_2] * K_{BL} * [BL] * \omega_{Cat.}}{(K_{BL} * [BL] + K_{BHP} * [BHP] + 1)}$
Non-competitive Langmuir Hinshelwood with no dissociation of hydrogen (NCLH1)	$\frac{k_1 * K_{H2} * [H_2]}{(1 + K_{H2} * [H_2])} * \frac{K_{BL^\wedge} * [BL]}{(1 + K_{BHP^\wedge} * [BHP] + K_{BL^\wedge} * [BL])} * \omega_{Cat.}$
Non-competitive Langmuir Hinshelwood with hydrogen dissociation (NCLH2)	$\frac{k_1 * K_H * K_C * K_{BL^\wedge} * [H_2]}{\sqrt{K_H * [H_2]} + 1} * \frac{[BL] * \omega_{Cat.}}{K_{BL^\wedge}.[BL] + K_C.\sqrt{K_H * [H_2]}.K_{BL^\wedge}.[BL]. + K_{BHP^\wedge}.[BHP] + 1}$

The terms K_{BL}, K_{H2}, K_H, $K_{BL^\wedge}$, $K_{BHP^\wedge}$ and K_{BHP} are adsorption constants. The term K_i and K_C are equilibrium constants. The term $\omega_{Cat.}$ is the catalyst loading (mass of dried basis per reaction volume). For the cyclization step, two options must be considered: non-catalytic and heterogeneous catalytic one. The non-catalytic one is expressed as

$$R_{2,non-cat.} = k_{2,non-cat.} * [BHP] \quad (1)$$

The rate of a heterogeneously catalytic reaction was also supposed to be the first order in the reactant

$$R_{2,Heterogeneous} = k_{2,Heterogeneous} * [BHP] * \omega_{Cat.} \quad (2)$$

For each mechanism, two options were considered, one comprising only non-catalytic contribution and the other one considering both non-catalytic and catalytic cyclization (Table 3).

Table 3. Tested models for the hydrogenation of BL to GVL.

	HYDROGENATION STEP					**CYCLIZATION STEP**	
	LH1	**LH2**	**ER1**	**NCLH1**	**NCLH2**	**Non-catalyzed**	**Heterogeneous catalyst**
Model 1	X					X	
Model 2	X					X	X
Model 3		X				X	
Model 4		X				X	X
Model 5			X			X	
Model 6			X			X	X
Model 7				X		X	
Model 8				X		X	X
Model 9					X	X	
Model 10					X	X	X

3.2.2 Material balances

Kinetic experiments were carried out under isobaric and isothermal conditions. A previous study[34] found that external and internal mass transfer limitations can be assumed to be negligible under the current operating conditions.

Material balances for the different compounds in the liquid phase can be expressed as:

$$\frac{dC_{BL}}{dt} = -R_1 \quad (3)$$

$$\frac{d[H_2]_{liq}}{dt} = k_L.a * \left([H_2]^*_{liq} - [H_2]_{liq}\right) - R_1 \quad (4)$$

$$\frac{dC_{BHP}}{dt} = R_1 - R_{2,non-cat} - R_{2,Heterogeneous} \quad (5)$$

$$\frac{dC_{BuOH}}{dt} = R_{2,non-cat} + R_{2,Heterogeneous} \quad (6)$$

$$\frac{dC_{GVL}}{dt} = R_{2,non-cat} + R_{2,Heterogeneous} \quad (7)$$

In eq 4, $[H_2]^*_{liq}$ reflects the concentration of hydrogen at the gas-liquid interface. The values of this term were determined through Henry's constant in GVL as a solvent $He(T) = \frac{[H_2]^*_{liq}}{P_{H_2,Reactor}}$ [34]. In this study, the values of $k_L.a$, i.e., volumetric gas to liquid mass transfer coefficient for hydrogen was expressed as a function of density, viscosity and temperature [42].

3.2.3 Parameter estimation

Two observables were used: concentrations of BL and BHP. The commercial software Athena Visual Studio, using the Bayesian statistics, was used to develop the models [49,50].

The concentrations of BL and BHP were used as observables during the parameter estimation stage. Several studies demonstrated that the Bayesian framework is better for the multi-response parameter estimation than the method of non-linear least squares [51,52]. Such approach started to be widely applied in the kinetic modeling of several catalytic systems [51,53–63].

The ordinary differential equations (ODEs) are solved by DDAPLUS, which solves non-linear initial-value problems involving stiff implicit systems. GREGPLUS package was used for the parameter estimation stage.

The probability of the model M_ω, describing the experimental concentrations Y within the error space $\sum$, was calculated [49,50]. This probability, $p(M_\omega|Y,\sum)$, is known as the posterior distribution and is calculated as:

$$p(M_\omega|Y,\sum) = \frac{L(Y,\ \sum|M_\omega)\cdot p(M_\omega)}{C} \quad (8)$$

where, $L(Y,\ \sum|M_\omega)$ is the likelihood function evaluating the probability of the experimental concentrations Y generated by the model M_ω with its parameter vector θ. The term C is a normalization constant. The probability $p(M_\omega)$ is the prior distribution taking into account the experimentalist knowledge. The boundaries of the estimated parameters are known, and the error space is evaluated by replicate experiments.

The model discrimination was evaluated by the determination of the normalized posterior probabilities (eq 9).

$$\pi(M_k|Y,\Sigma) = \frac{p(M_k|Y,\Sigma)*100}{\sum_k p(M_k|Y,\Sigma)} \quad (9)$$

During the parameter estimation, the GREGPLUS package minimizes the objective function $S(\theta)$, and can calculate the maximum posterior probability density of the different estimated parameters θ and the values of the posterior distribution of the tested models [49,50].

$$S(\theta) = (n + m + 1) \cdot ln|v(\theta)| \quad (10)$$

where, n is the number of events in response, m is the number of responses and $|v(\theta)|$ is the determinant of the covariance matrix of the responses. Each element of this matrix is defined as:

$$v_{ij}(\theta) = \sum_{u=1}^{n}[Y_{iu} - f_{iu}(\xi_u, \theta)] \cdot \left[Y_{ju} - f_{ju}(\xi_u, \theta)\right] \quad (11)$$

with Y_{iu} the experimental concentration and $f_{iu}(\xi_u, \theta)$ the estimated value for the response i and event u; Y_{ju} the experimental concentration and $f_{ju}(\xi_u, \theta)$ the estimated value for response j and event u.

The precision of the estimated parameters was evaluated by the marginal highest posterior density (HPD). The 95% HPD was calculated by the GREGPLUS package.

The parameters to be estimated are the adsorption constants, the rate constants and the activation energies.

The modified Arrhenius equation is used in order to decrease the correlation between the pre-exponential factor and the activation energy:

$$k_i(T_R) = k_i(T_{ref}) \cdot \exp\left(-\frac{E_{a_i}}{T_R}\left(\frac{1}{T_R} - \frac{1}{T_{ref}}\right)\right) \quad (12)$$

where, T_{ref} is the reference temperature (T_{ref}=403.15K) chosen in the considered experimental temperature range.

3.2.4 Results

Preliminary modeling results show that the adsorption constant for the intermediate BHP was close to zero, and that the ring-closure reaction catalyzed by Ru/C did not exhibit any temperature dependence. Thus, $Ea_{2,\,heterogeneous}$ was set to 0 kJ/mol. These preliminary results motivate our choice to not consider these two kinetic constants in the modeling stage.

Tables 4 shows the value of the posterior probability share for each model. One can notice that Model 8 (41.35%), 2 (31.80%) and 4 (22.26%) are the most probable ones. For that reason, the modeling output for these three models are discussed and presented in the following. Due to space limitation, the parity plots for these models are included in Supporting Information (Figures S1-S3). The parity plots show that the fitting quality of the three models is good. One should also observe that it is impossible to discriminate the most probable model only from the parity plots. Indeed, the R2 values are similar from these three models.

The effect of the number of estimated parameters on the models was evaluated via the AIC number standing for Akaike Information Criterion (Table 4).[64]

$$AIC = number\ of\ independant\ event \cdot ln\left(\frac{\left[Y_{ju} - f_{ju}(\xi_u, \theta)\right]^2}{number\ of\ independant\ event}\right) + 2 \cdot Number\ of\ estimated\ parameters \quad (13)$$

The model with the lowest AIC value is of best quality. From Table 4, it can be concluded that Models 4 and 8 have the lowest AIC value, than Model 2.

Table 4. Modeling results from Bayesian statistics.

Model	Objective function $S(\theta)$	Posterior probability $\text{Log}_{10}\, p(M_k \mid Y, \Sigma)$	Posterior probability share $\pi(M_k \mid Y, \Sigma)$ in%	Number of estimated parameters	AIC
1	6497.91	-1.25 10^{+2}	0.08	6	4.27E+03
2	6430.30	-1.22 10^{+2}	31.80	7	4.16E+03
3	6451.40	-1.25 10^{+2}	0.06	7	4.26E+03
4	6386.27	-1.22 10^{+2}	22.26	7	4.15E+03
5	6647.54	-1.27 10^{+2}	0.00	4	4.42E+03
6	6602.22	-1.26 10^{+2}	0.01	5	4.35E+03
7	6464.54	-1.25 10^{+2}	0.09	6	4.26E+03
8	6417.32	-1.22 10^{+2}	41.35	6	4.15E+03
9	8114.67	-1.50 10^{+2}	0.00	1	5.77E+03
10	6434.52	-1.23 10^{+2}	4.35	5	4.19E+03

Tables S1-S3 (Supporting Information) displaying correlations between the estimated parameters illustrate significant correlations between the rate constant $k_1(Tref)$ and the adsorption constants. For Models 2 and 4, the rate constant $k_1(Tref)$ and the adsorption constants (K_{H2} and K_{BL}) are in particular correlated, reflecting difficulties in the determination of adsorption constants directly from kinetic data.

Tables 5-7 show the estimated values and their HPD intervals for the three models.

From Model 2 (Table 5), the HDP interval is quite essential for the estimation of K_{BL}. The estimation of such adsorption constant can be difficult.

Table 5. Estimated values at T_{ref}=403.15K and statistical data for Model 2.

		Bayesian approach	
Parameters	Units	Estimated	HPD Intervals %
$k_1(Tref)$	mol/s/kg_dry basis cat	3.57	68.18
Ea_1	J/mol	33094.04	13.42
K_{H2}	m^3/mol	0.0439	29.65
K_{BL}	m^3/mol	$2.78\ 10^{-4}$	80.23
$k_{2,Het}(Tref)$	m^3/s/kg_dry basis cat	3.7210^{-6}	23.80
$k_{2,non-cat}(Tref)$	1/s	$2.15\ 10^{-5}$	18.14
$Ea_{2,non-cat}$	J/mol	$3.07\ 10^{4}$	43.12

The parameter estimation for Model 4 was less accurate (Table 6). The HDP intervals for $k_1(T_{ref})$, K_{H2} and K_{BL} are higher than 100%.

Table 6. Estimated values at T_{ref}=403.15K and statistical data for Model 4.

		Bayesian approach	
Parameters	Units	Estimated	HPD Intervals %
$k_1(Tref)$	mol/m^3/s/kg_dry basis cat	40.4	>100%
Ea_1	J/mol	3.05 10^4	12.88
K_{H2}	m^3/mol	29.0	>100%
K_{BL}	m^3/mol	4.31 10^{-03}	>100%
K_i	-	nd	nd
$k_{2,Het}(Tref)$	m^3/s/kg_dry basis cat	3.67 10^{-06}	24.19
$k_{2,non-cat}(Tref)$	1/s	2.20 10^{-05}	17.46
$Ea_{2,non-cat}$	J/mol	2.86 10^{04}	43.83

The confidence intervals presented in Table 7 displaying the estimated values for Model 8 show reliability of such estimates.

Table 7. Estimated values et T_{ref}=403.15K and statistical data for Model 8.

		Bayesian approach	
Parameters	Units	Estimated	HPD Intervals %
$k_1(Tref)$	mol/m^3/s/kg_dry basis cat	0.711	52.72
Ea_1	J/mol	29472.46	14.69
K_{H2}	m^3/mol	0.264	39.59
K_{BL}^	m^3/mol	3.94 10^{-04}	63.86
$k_{2,Het}(Tref)$	m^3/s/kg_dry basis cat	3.67 10^{-06}	24.05
$k_{2,non-cat}(Tref)$	1/s	2.20 10^{-05}	9.38
$Ea_{2,non-cat}$	J/mol	28661.77	43.65

The estimated parameters from Model 4 exhibit rather important uncertainties; therefore the calculations are displayed only for Models 2 and 8.

Although description of the experimental data by Model 2 is quite good (Figure S1), the correspondence for the intermediate compound is worse than for BL. Figure 6 shows the data fitting results of some experiments (entries 5, 7, 8, 9 and 11 in Table 1) with the Bayesian approach. It follows from the calculations that the Model 2 tends to slightly overestimate the concentration of the intermediate for experiment 7 (Table 1).

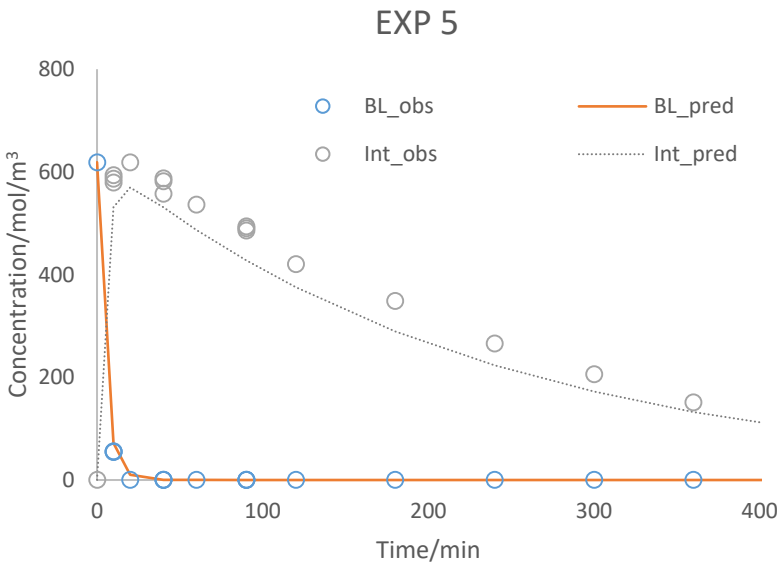

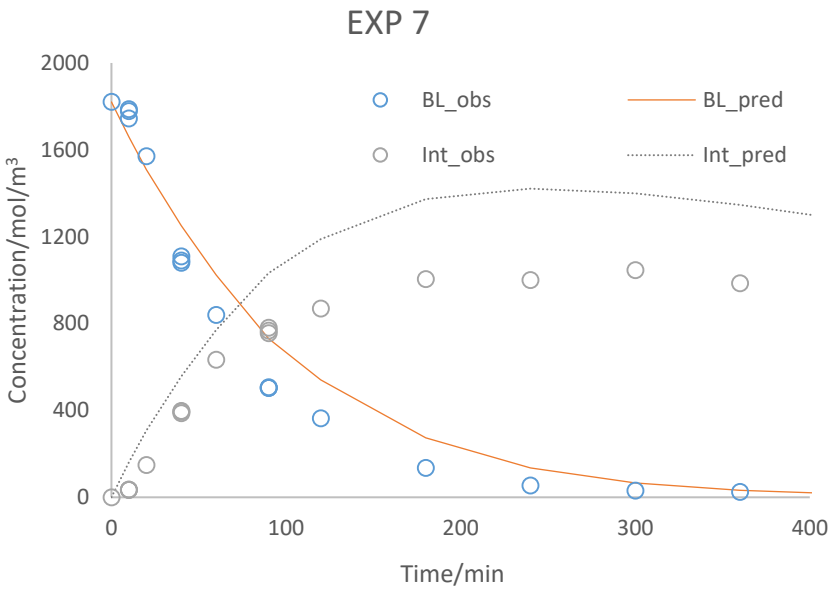
EXP 7
2000
1600
1200
800
400
0
Concentration/mol/m³
0
100
200
300
400
Time/min
BL_obs
BL_pred
Int_obs
Int_pred

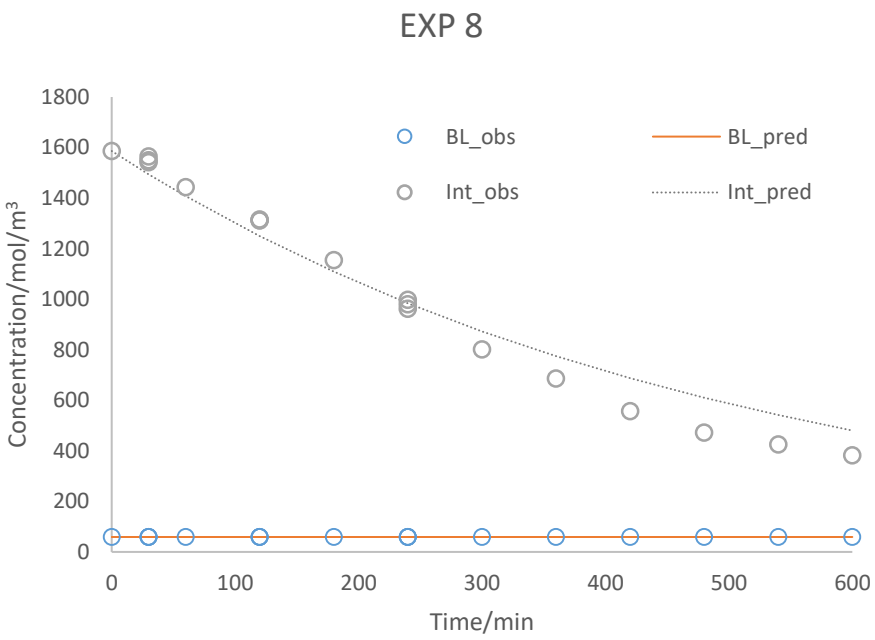
EXP 8
1800
1600
1400
1200
1000
800
600
400
200
0
Concentration/mol/m³
0
100
200
300
400
500
600
Time/min
BL_obs
BL_pred
Int_obs
Int_pred

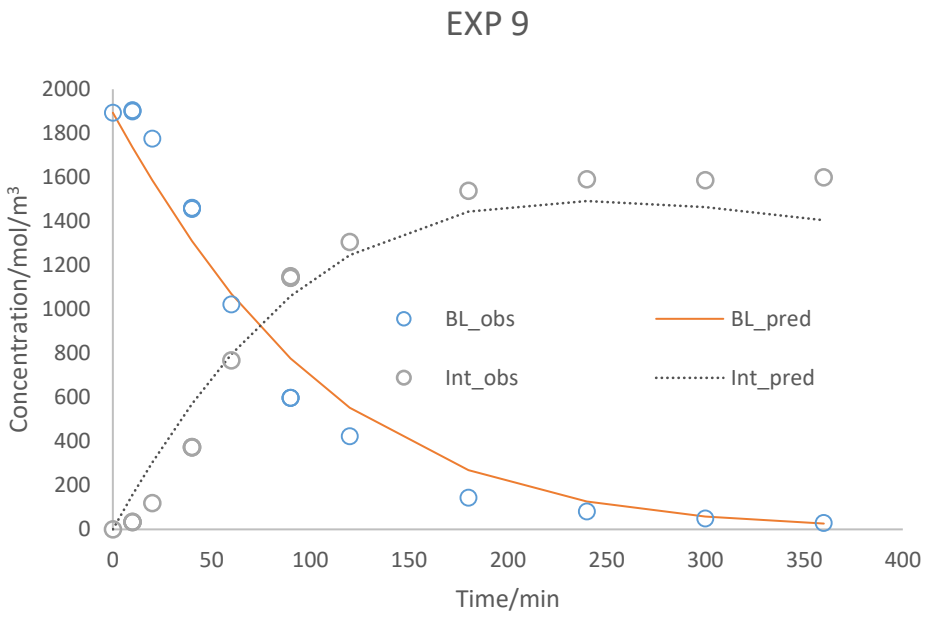
EXP 9
Concentration/mol/m³
2000
1800
1600
1400
1200
1000
800
600
400
200
0
0
50
100
150
200
250
300
350
400
Time/min
BL_obs
BL_pred
Int_obs
Int_pred

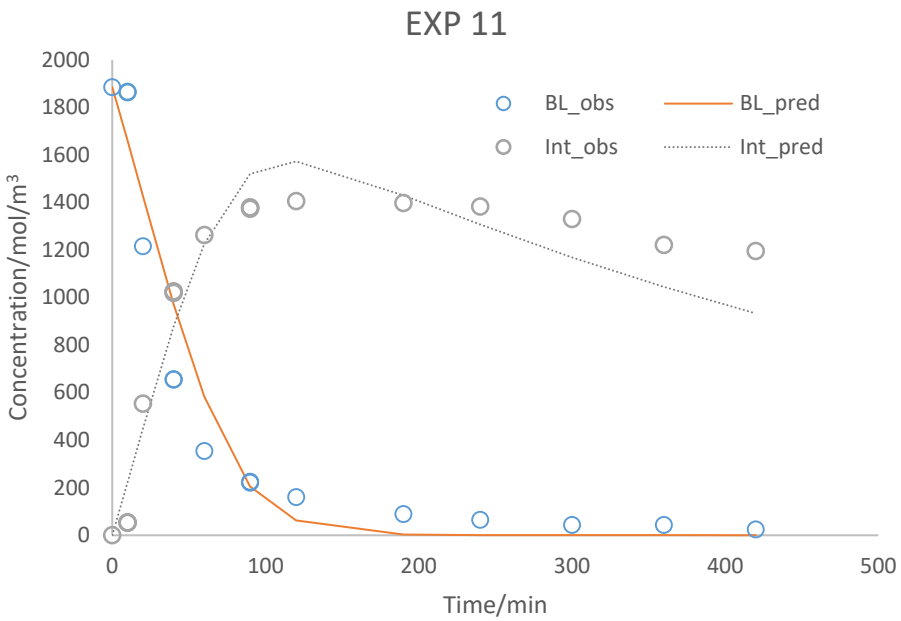

Figure 6. Fit of Model 2 (Langmuir-Hinshelwood with molecular adsorption of H_2) to the experimental concentrations. EXP 5 (P_{H2}: 22.3 bar, Temp: 427.15 K, m_{cat} (50wt% moisture): 0.0028 kg, $[BL]_0$: 619 mol/m^3, $[GVL]_0$: 8827 mol/m^3 and $[Interm]_0=[BuOH]_0$= 0 mol/m^3); EXP 7 (P_{H2}: 23.8 bar, Temp: 373.2 K, m_{cat} (50wt% moisture): 0.0005 kg, $[BL]_0$: 1821 mol/m^3, $[GVL]_0$: 6851 mol/m^3 and $[Interm]_0=[BuOH]_0$= 0 mol/m^3); EXP 8 (P_{H2}: 23.3 bar, Temp: 423.15 K, m_{cat} (50wt% moisture): 0.0000 kg, $[BL]_0$: 59 mol/m^3, $[GVL]_0$: 6884 mol/m^3, $[Interm]_0$=1586 mol/m^3 and $[BuOH]_0$= 189 mol/m^3); EXP 9 (P_{H2}: 16.3 bar, Temp: 373.15 K, m_{cat} (50wt% moisture): 0.0005 kg, $[BL]_0$: 1893 mol/m^3, $[GVL]_0$: 6719 mol/m^3 and $[Interm]_0=[BuOH]_0$= 0 mol/m^3) and EXP 11 (P_{H2}: 5.2 bar, Temp: 393.15 K, m_{cat} (50wt% moisture): 0.0010 kg, $[BL]_0$: 1885 mol/m^3, $[GVL]_0$: 6720 mol/m^3 and $[Interm]_0=[BuOH]_0$= 0 mol/m^3).

Visually, the fitting of Model 8 (Figure 7) is very similar to Model 2 having a slightly better fit even if the concentration of intermediates for experiment 7 is also overestimated. The uncertainty for the estimated parameters of Model 8 was lower compared to the Model 2.

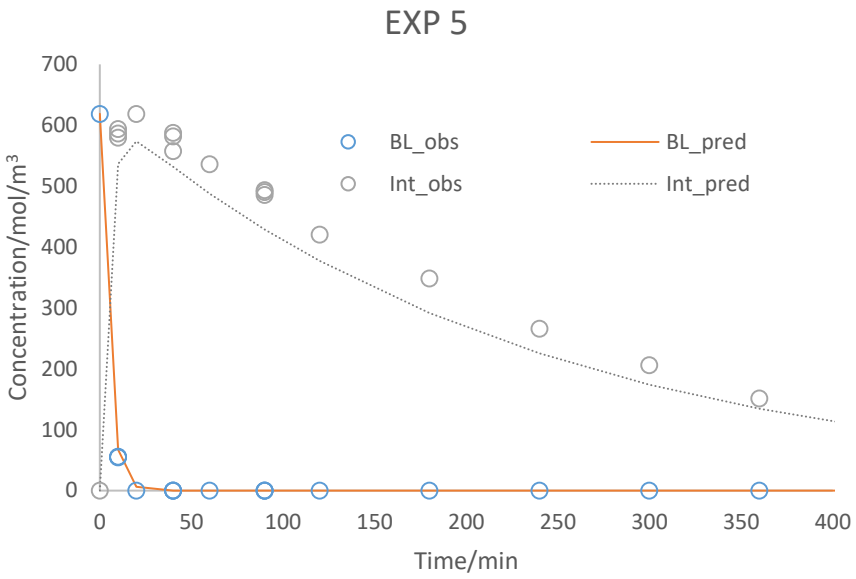
EXP 5
Concentration/mol/m³
Time/min
BL_obs
Int_obs
BL_pred
Int_pred
0
100
200
300
400
500
600
700
0
50
100
150
200
250
300
350
400

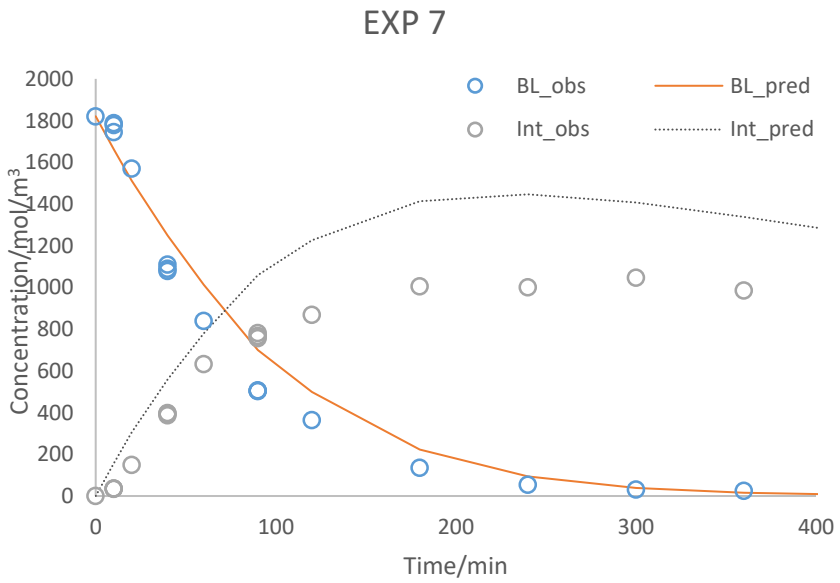
EXP 7
Concentration/mol/m³
Time/min
BL_obs
Int_obs
BL_pred
Int_pred
0
200
400
600
800
1000
1200
1400
1600
1800
2000
0
100
200
300
400

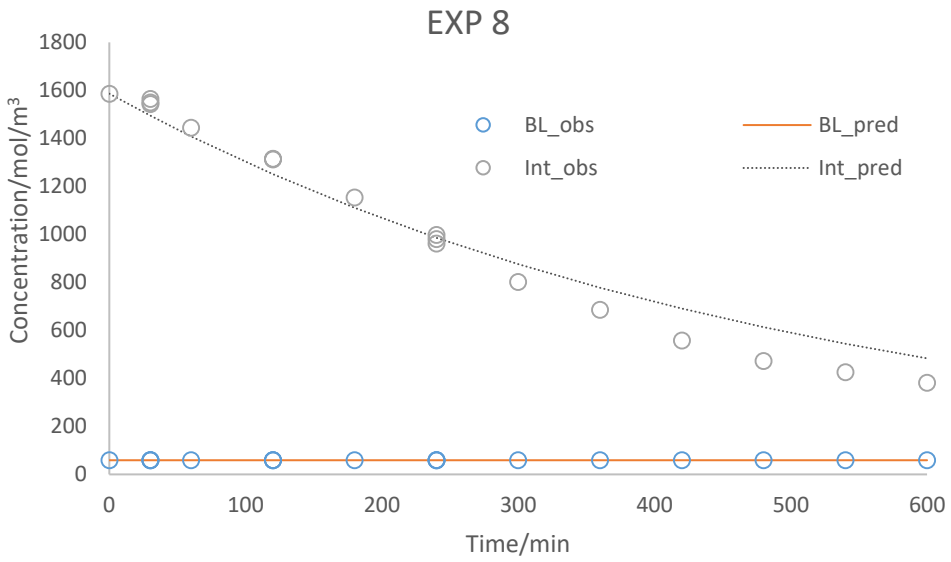
EXP 8
Concentration/mol/m³
1800
1600
1400
1200
1000
800
600
400
200
0
0
100
200
300
400
500
600
Time/min
BL_obs
Int_obs
BL_pred
Int_pred

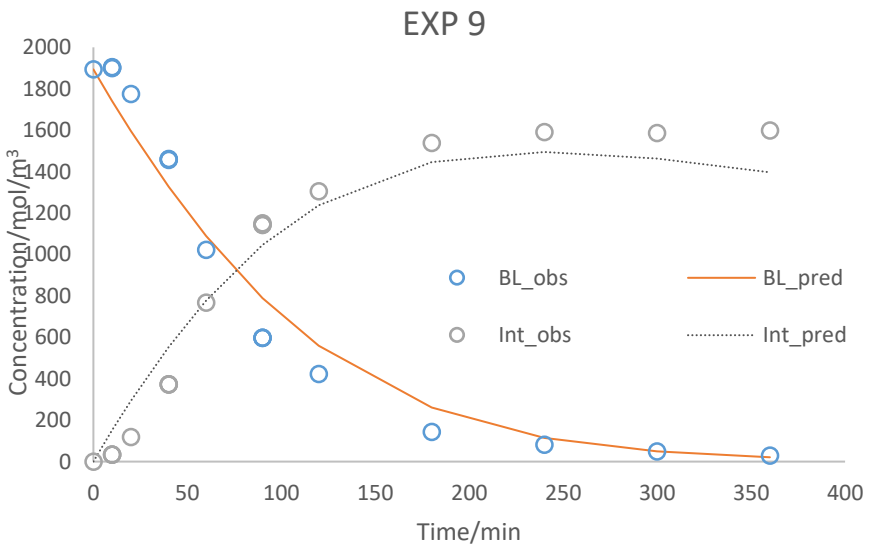
EXP 9
Concentration/mol/m³
2000
1800
1600
1400
1200
1000
800
600
400
200
0
0
50
100
150
200
250
300
350
400
Time/min
BL_obs
Int_obs
BL_pred
Int_pred

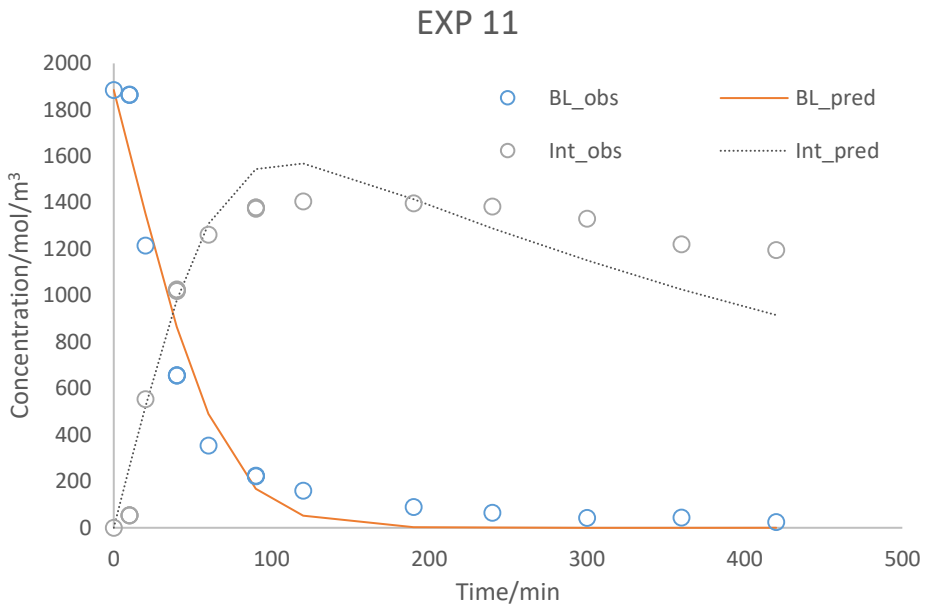

Figure 7. Fit of Model 8 (Non-competitive Langmuir-Hinshelwood with no dissociation of hydrogen) to the experimental concentrations. EXP 5 (P_{H2}: 22.3 bar, Temp: 427.15 K, m_{cat} (50wt% moisture): 0.0028 kg, $[BL]_0$: 619 mol/m^3, $[GVL]_0$: 8827 mol/m^3 and $[Interm]_0=[BuOH]_0$= 0 mol/m^3); EXP 7 (P_{H2}: 23.8 bar, Temp: 373.2 K, m_{cat} (50wt% moisture): 0.0005 kg, $[BL]_0$: 1821 mol/m^3, $[GVL]_0$: 6851 mol/m^3 and $[Interm]_0=[BuOH]_0$= 0 mol/m^3); EXP 8 (P_{H2}: 23.3 bar, Temp: 423.15 K, m_{cat} (50wt% moisture): 0.0000 kg, $[BL]_0$: 59 mol/m^3, $[GVL]_0$: 6884 mol/m^3, $[Interm]_0$=1586 mol/m^3 and $[BuOH]_0$= 189 mol/m^3); EXP 9 (P_{H2}: 16.3 bar, Temp: 373.15 K, m_{cat} (50wt% moisture): 0.0005 kg, $[BL]_0$: 1893 mol/m^3, $[GVL]_0$: 6719 mol/m^3 and $[Interm]_0=[BuOH]_0$= 0 mol/m^3) and EXP 11 (P_{H2}: 5.2 bar, Temp: 393.15 K, m_{cat} (50wt% moisture): 0.0010 kg, $[BL]_0$: 1885 mol/m^3, $[GVL]_0$: 6720 mol/m^3 and $[Interm]_0=[BuOH]_0$= 0 mol/m^3).

4. Conclusion

Production of γ-valerolactone (GVL) from the hydrogenation of alkyl levulinate over Ru/C is investigated more and more because GVL is a promising platform molecule. The use of butyl levulinate (BL) instead of levulinic acid present two benefits: decrease of corrosion and low vapor pressure of the reaction mixture. The reaction mechanism for this reaction is still under debate; for that reason, Bayesian inference was used. The hydrogenation of BL over Ru/C in GVL solvent was studied.

Kinetic experiments were performed in an autoclave under isothermal and isobaric conditions. Different kinetic models were evaluated: Langmuir-Hinshelwood (LH) with molecular adsorption of H_2, LH with hydrogen dissociation, Eley-Rideal with no adsorption of hydrogen, non-competitive LH with no dissociation of hydrogen and non-competitive LH with hydrogen dissociation. For each evaluated model, the catalyzed effect of Ru/C on the cyclization was evaluated.

It was found that the catalyst Ru/C catalyzes the cyclization reaction step. Based on the posterior probability and AIC evaluation, the non-competitive LH with no dissociation of hydrogen, including the second reaction heterogeneously catalyzed, is the most probable reaction mechanism. This model was shown to be correct for a reaction temperature range 373.15-427.15 K, a hydrogen pressure range 5.2-23.8 bar, BL concentration range 56-1893 mol/m^3 and a catalyst mass 0.00-0.0028 kg (50wt% moisture). This work highlights the benefits of using Bayesian inference to evaluate the most probable models. A continuation of this work could be to test different activated carbon support with different acid site concentrations to have a better understanding of the ring-closure reaction catalyzed by the support.

Abbreviation

D_j	molecular diffusion coefficient of *j* [$m^2.s^{-1}$]
Ea_i	activation energy of reaction *i* [$J.mol^{-1}$]
He	Henry's coefficient [$mol.m^{-3}.bar^{-1}$]
ΔH_{sol}	dissolution enthalpy [$J.mol^{-1}$]
k_i	Rate constant of reaction *i*
$k_L.a$	volumetric mass transfer coefficient [s^{-1}]
$(k_L.a)_{modified}$	modified volumetric mass transfer coefficient [$\left(\frac{Pa.s}{K}\right)^{0.5} . \left(\frac{Pa.s}{kg.m^{-3}}\right)^{0.25} . s^{-1}$]
r_j	rate of formation or disappearance of compound *j* [$mol.m^{-3}.s^{-1}$]
P	pressure [bar]
R_i	reaction rate *i* [$mol.m^{-3}.s^{-1}$]
R	gas constant [$J.K^{-1}.mol^{-1}$]
R^2	coefficient of explanation [%]
T	temperature [K]
V_{molar}	molar volume [$cm^3.mol^{-1}$]
w_i	weight percent
y_i	experimental observable
$\bar{y}$	mean value of the experimental observables
$\hat{y}_i$	observable simulated by the model

Greek letters

δ	sensitivity factor of a reaction series to steric effects
μ	liquid viscosity [Pa.s]
ρ	mass density [kg.m^{-3}]
ω	objective function
$\omega_{Cat.}$	catalyst loading [kg_dried basis.m^{-3}]

Subscripts and superscripts

ave	average
Ref	reference
*	interfacial value

Abbreviations

AIC	akaike information criterion
BL	butyl levulinate
BHP	butyl 4-hydroxypentanoate
BuOH	butanol
GVL	γ-valerolactone
ROH	co-product of the second reaction (butanol)

Associated Content

Supporting Information.

Supporting information consists of additional information on: Derivation of rate constants, Parity plots and Correlation matrix.

Author Information

Corresponding Author

Sébastien Leveneur[*1]

[1]Laboratoire de Sécurité des Procédés Chimiques, Institut National des Sciences Appliquées de Rouen, 76800 Saint-Étienne-du-Rouvray, France. Email: sebastien.leveneur@insa-rouen.fr

Acknowledgments

This study has been done in the framework of Task 2: “Green process: 2nd generation of biomass” of AMED project. The authors thank the AMED project. The AMED project has been funded with the support from the European Union with the European Regional Development Fund (ERDF) and from the Regional Council of Normandie. For the analytical part (GC-FID), the authors thank the European Regional Development Fund (GreenChem) and the Laboratoire d’Excellence (LabEx) SynOrg (ANR-11-LABX-0029). The authors thank the Maîtrise des Risques et Environementaux department, and the Erasmus program to make the research project of Sarah Capecci possible.

References

(1) Liu, W.; Xu, J.; Xie, X.; Yan, Y.; Zhou, X.; Peng, C. A New Integrated Framework to Estimate the Climate Change Impacts of Biomass Utilization for Biofuel in Life Cycle Assessment. *J. Clean. Prod.* **2020**, *267*. https://doi.org/10.1016/j.jclepro.2020.122061.

(2) Chandel, A. K.; Garlapati, V. K.; Jeevan Kumar, S. P.; Hans, M.; Singh, A. K.; Kumar, S. The Role of Renewable Chemicals and Biofuels in Building a Bioeconomy. *Biofuels, Bioprod. Biorefining* **2020**, *14* (4), 830–844. https://doi.org/10.1002/bbb.2104.

(3) Ventura, M.; Marinas, A.; Domine, M. E. Catalytic Processes for Biomass-Derived Platform Molecules Valorisation. *Top. Catal.* **2020**, *63*, 846–865. https://doi.org/10.1007/s11244-020-01309-9.

(4) Adeleye, A. T.; Louis, H.; Akakuru, O. U.; Joseph, I.; Enudi, O. C.; Michael, D. P. A Review on the Conversion of Levulinic Acid and Its Esters to Various Useful Chemicals. *AIMS Energy*. **2019**, *7(2)*, 165-185. https://doi.org/10.3934/ENERGY.2019.2.165.

(5) Yan, K.; Yang, Y.; Chai, J.; Lu, Y. Catalytic Reactions of Gamma-Valerolactone: A Platform to Fuels and Value-Added Chemicals. *Appl. Catal. B Environ.* **2015**, *179*, 292–304. https://doi.org/10.1016/j.apcatb.2015.04.030.

(6) Wright, W. R. H.; Palkovits, R. Development of Heterogeneous Catalysts for the Conversion of Levulinic Acid to γ-Valerolactone. *ChemSusChem* **2012**, *5* (9), 1657–1667. https://doi.org/10.1002/cssc.201200111.

(7) Alonso, D. M.; Wettstein, S. G.; Dumesic, J. A. Gamma-Valerolactone, a Sustainable Platform Molecule Derived from Lignocellulosic Biomass. *Green Chem.* **2013**, *15* (3), 584–

595. https://doi.org/10.1039/C3GC37065H.

(8) Tang, X.; Zeng, X.; Li, Z.; Hu, L.; Sun, Y.; Liu, S.; Lei, T.; Lin, L. Production of γ-Valerolactone from Lignocellulosic Biomass for Sustainable Fuels and Chemicals Supply. *Renew. Sustain. Energy Rev.* **2014**, *40*, 608–620. https://doi.org/10.1016/j.rser.2014.07.209.

(9) Al-Shaal, M. G.; Wright, W. R. H.; Palkovits, R. Exploring the Ruthenium Catalysed Synthesis of γ-Valerolactone in Alcohols and Utilisation of Mild Solvent-Free Reaction Conditions. *Green Chem.* **2012**, *14* (5), 1260–1263. https://doi.org/10.1039/C2GC16631C.

(10) Du, X.; Liu, Y.; Wang, J.; Cao, Y.; Fan, K. Catalytic Conversion of Biomass-Derived Levulinic Acid into γ-Valerolactone Using Iridium Nanoparticles Supported on Carbon Nanotubes. *Chinese J. Catal.* **2013**, *34* (5), 993–1001. https://doi.org/10.1016/S1872-2067(11)60522-6.

(11) Xu, H.; Hu, D.; Zhang, M.; Wang, Y.; Zhao, Z.; Jiang, Z.; Garces, H. F.; Yan, K. Bimetallic NiCu Alloy Catalysts for Hydrogenation of Levulinic Acid. *ACS Appl. Nano Mater.* **2021**, *4* (4), 3989–3997. https://doi.org/10.1021/acsanm.1c00339.

(12) Hengne, A. M.; Rode, C. V. Cu–ZrO2 Nanocomposite Catalyst for Selective Hydrogenation of Levulinic Acid and Its Ester to γ-Valerolactone. *Green Chem.* **2012**, *14* (4), 1064–1072. https://doi.org/10.1039/C2GC16558A.

(13) Luo, W.; Deka, U.; Beale, A. M.; van Eck, E. R. H.; Bruijnincx, P. C. A.; Weckhuysen, B. M. Ruthenium-Catalyzed Hydrogenation of Levulinic Acid: Influence of the Support and Solvent on Catalyst Selectivity and Stability. *J. Catal.* **2013**, *301*, 175–186. https://doi.org/10.1016/j.jcat.2013.02.003.

(14) Mehdi, H.; Fábos, V.; Tuba, R.; Bodor, A.; Mika, L. T.; Horváth, I. T. Integration of Homogeneous and Heterogeneous Catalytic Processes for a Multi-Step Conversion of Biomass: From Sucrose to Levulinic Acid, γ-Valerolactone, 1,4-Pentanediol, 2-Methyl-Tetrahydrofuran, and Alkanes. *Top. Catal.* **2008**, *48* (1), 49–54. https://doi.org/10.1007/s11244-008-9047-6.

(15) Park, J. Y.; Kim, M. A.; Lee, S. J.; Jung, J.; Jang, H. M.; Upare, P. P.; Hwang, Y. K.; Chang, J.-S.; Park, J. K. Preparation and Characterization of Carbon-Encapsulated Iron Nanoparticles and Their Catalytic Activity in the Hydrogenation of Levulinic Acid. *J. Mater. Sci.* **2015**, *50* (1), 334–343. https://doi.org/10.1007/s10853-014-8592-6.

(16) Shimizu, K.; Kanno, S.; Kon, K. Hydrogenation of Levulinic Acid to γ-Valerolactone by Ni and MoOx Co-Loaded Carbon Catalysts. *Green Chem.* **2014**, *16* (8), 3899–3903. https://doi.org/10.1039/C4GC00735B.

(17) Sudhakar, M.; Lakshmi Kantam, M.; Swarna Jaya, V.; Kishore, R.; Ramanujachary, K. V; Venugopal, A. Hydroxyapatite as a Novel Support for Ru in the Hydrogenation of Levulinic Acid to γ-Valerolactone. *Catal. Commun.* **2014**, *50*, 101–104. https://doi.org/10.1016/j.catcom.2014.03.005.

(18) Testa, M. L.; Corbel-Demailly, L.; La Parola, V.; Venezia, A. M.; Pinel, C. Effect of Au on Pd Supported over HMS and Ti Doped HMS as Catalysts for the Hydrogenation of Levulinic Acid to γ-Valerolactone. *Catal. Today* **2015**, *257*, 291–296. https://doi.org/10.1016/j.cattod.2014.06.009.

(19) Abdelrahman, O. A.; Heyden, A.; Bond, J. Q. Analysis of Kinetics and Reaction Pathways in the Aqueous-Phase Hydrogenation of Levulinic Acid to Form γ-Valerolactone over Ru/C.

ACS Catal. **2014**, *4* (4), 1171–1181. https://doi.org/10.1021/cs401177p.

(20) Son, P. A.; Nishimura, S.; Ebitani, K. Production of γ-Valerolactone from Biomass-Derived Compounds Using Formic Acid as a Hydrogen Source over Supported Metal Catalysts in Water Solvent. *RSC Adv.* **2014**, *4* (21), 10525–10530. https://doi.org/10.1039/C3RA47580H.

(21) Yuan, J.; Li, S.-S.; Yu, L.; Liu, Y.-M.; Cao, Y.; He, H.-Y.; Fan, K.-N. Copper-Based Catalysts for the Efficient Conversion of Carbohydrate Biomass into γ-Valerolactone in the Absence of Externally Added Hydrogen. *Energy Environ. Sci.* **2013**, *6* (11), 3308–3313. https://doi.org/10.1039/C3EE40857D.

(22) Deng, L.; Li, J.; Lai, D.-M.; Fu, Y.; Guo, Q.-X. Catalytic Conversion of Biomass-Derived Carbohydrates into γ-Valerolactone without Using an External H2 Supply. *Angew. Chemie Int. Ed.* **2009**, *48* (35), 6529–6532. https://doi.org/10.1002/anie.200902281.

(23) Deng, L.; Zhao, Y.; Li, J.; Fu, Y.; Liao, B.; Guo, Q.-X. Conversion of Levulinic Acid and Formic Acid into γ-Valerolactone over Heterogeneous Catalysts. *ChemSusChem* **2010**, *3* (10), 1172–1175. https://doi.org/10.1002/cssc.201000163.

(24) Fábos, V.; Mika, L. T.; Horváth, I. T. Selective Conversion of Levulinic and Formic Acids to γ-Valerolactone with the Shvo Catalyst. *Organometallics* **2014**, *33* (1), 181–187. https://doi.org/10.1021/om400938h.

(25) Fellay, C.; Dyson, P. J.; Laurenczy, G. A Viable Hydrogen-Storage System Based On Selective Formic Acid Decomposition with a Ruthenium Catalyst. *Angew. Chemie Int. Ed.* **2008**, *47* (21), 3966–3968. https://doi.org/10.1002/anie.200800320.

(26) Heeres, H.; Handana, R.; Chunai, D.; Rasrendra, C. B.; Girisuta, B.; Heeres, H. J. Combined Dehydration/(Transfer)-Hydrogenation of C6-Sugars (D-Glucose and D-Fructose) to γ-Valerolactone Using Ruthenium Catalysts. *Green Chem.* **2009**, *11* (8), 1247–1255. https://doi.org/10.1039/B904693C.

(27) Hengne, A. M.; Malawadkar, A. V; Biradar, N. S.; Rode, C. V. Surface Synergism of an Ag–Ni/ZrO2 Nanocomposite for the Catalytic Transfer Hydrogenation of Bio-Derived Platform Molecules. *RSC Adv.* **2014**, *4* (19), 9730–9736. https://doi.org/10.1039/C3RA46495D.

(28) Ortiz-Cervantes, C.; García, J. J. Hydrogenation of Levulinic Acid to γ-Valerolactone Using Ruthenium Nanoparticles. *Inorganica Chim. Acta* **2013**, *397*, 124–128. https://doi.org/10.1016/j.ica.2012.11.031.

(29) Ruppert, A. M.; Jędrzejczyk, M.; Sneka-Płatek, O.; Keller, N.; Dumon, A. S.; Michel, C.; Sautet, P.; Grams, J. Ru Catalysts for Levulinic Acid Hydrogenation with Formic Acid as a Hydrogen Source. *Green Chem.* **2016**, *18* (7), 2014–2028. https://doi.org/10.1039/C5GC02200B.

(30) Chia, M.; Dumesic, J. A. Liquid-Phase Catalytic Transfer Hydrogenation and Cyclization of Levulinic Acid and Its Esters to γ-Valerolactone over Metal Oxide Catalysts. *Chem. Commun.* **2011**, *47* (44), 12233–12235. https://doi.org/10.1039/C1CC14748J.

(31) Li, H.; Fang, Z.; Yang, S. Direct Catalytic Transformation of Biomass Derivatives into Biofuel Component γ-Valerolactone with Magnetic Nickel–Zirconium Nanoparticles. *Chempluschem* **2016**, *81* (1), 135–142. https://doi.org/10.1002/cplu.201500492.

(32) Li, H.; Fang, Z.; Yang, S. Direct Conversion of Sugars and Ethyl Levulinate into γ-

Valerolactone with Superparamagnetic Acid–Base Bifunctional ZrFeOx Nanocatalysts. *ACS Sustain. Chem. Eng.* **2016**, *4* (1), 236–246. https://doi.org/10.1021/acssuschemeng.5b01480.

(33) Simakova, I. L.; Demidova, Y. S.; Simonov, M. N.; Niphadkar, P. S.; Bokade, V. V.; Devi, N.; Dhepe, P. L.; Murzin, D. Y. Mesoporous Carbon and Microporous Zeolite Supported Ru Catalysts for Selective Levulinic Acid Hydrogenation into γ-Valerolactone. *Catal. Sustain. Energy* **2019**, *6*, 38–49. https://doi.org/10.1515/cse-2019-0004.

(34) Wang, Y.; Cipolletta, M.; Vernières-Hassimi, L.; Casson-Moreno, V.; Leveneur, S. Application of the Concept of Linear Free Energy Relationships to the Hydrogenation of Levulinic Acid and Its Corresponding Esters. *Chem. Eng. J.* **2019**, *374*, 822–831. https://doi.org/10.1016/j.cej.2019.05.218.

(35) Piskun, A. S.; van de Bovenkamp, H. H.; Rasrendra, C. B.; Winkelman, J. G. M.; Heeres, H. J. Kinetic Modeling of Levulinic Acid Hydrogenation to γ-Valerolactone in Water Using a Carbon Supported Ru Catalyst. *Appl. Catal. A Gen.* **2016**, *525*, 158–167. https://doi.org/10.1016/j.apcata.2016.06.033.

(36) Li, W.; Li, F.; Chen, J.; Betancourt, L. E.; Tu, C.; Liao, M.; Ning, X.; Zheng, J.; Li, R. Efficient and Sustainable Hydrogenation of Levulinic Acid to γ-Valerolactone in Aqueous Phase over Ru/MCM-49 Catalysts. *Ind. Eng. Chem. Res.* **2020**, *59* (39), 17338–17347. https://doi.org/10.1021/acs.iecr.0c01318.

(37) Kasar, G. B.; Medhekar, R. S.; Bhosale, P. N.; Rode, C. V. Kinetics of Hydrogenation of Aqueous Levulinic Acid over Bimetallic Ru-Ni/MMT Catalyst. *Ind. Eng. Chem. Res.* **2019**, *58* (43), 19803–19817. https://doi.org/10.1021/acs.iecr.9b03748.

(38) Protsenko, I. I.; Nikoshvili, L. Z.; Matveeva, V. G.; Sulman, E. M. Kinetic Modelling of Levulinic Acid Hydrogenation Over Ru-Containing Polymeric Catalyst. *Top. Catal.* **2020**, *63* (1–2), 243–253. https://doi.org/10.1007/s11244-020-01223-0.

(39) Wettstein, S. G.; Bond, J. Q.; Alonso, D. M.; Pham, H. N.; Datye, A. K.; Dumesic, J. A. RuSn Bimetallic Catalysts for Selective Hydrogenation of Levulinic Acid to γ-Valerolactone. *Appl. Catal. B Environ.* **2012**, *117–118*, 321–329. https://doi.org/10.1016/j.apcatb.2012.01.033.

(40) Zhang, L.; Mao, J.; Li, S.; Yin, J.; Sun, X.; Guo, X.; Song, C.; Zhou, J. Hydrogenation of Levulinic Acid into Gamma-Valerolactone over in Situ Reduced CuAg Bimetallic Catalyst: Strategy and Mechanism of Preventing Cu Leaching. *Appl. Catal. B Environ.* **2018**, *232*, 1–10. https://doi.org/10.1016/j.apcatb.2018.03.033.

(41) Negahdar, L.; Al-Shaal, M. G.; Holzhäuser, F. J.; Palkovits, R. Kinetic Analysis of the Catalytic Hydrogenation of Alkyl Levulinates to γ-Valerolactone. *Chem. Eng. Sci.* **2017**, *158*, 545–551. https://doi.org/10.1016/j.ces.2016.11.007.

(42) Ariba, H.; Wang, Y.; Devouge-Boyer, C.; Stateva, R. P.; Leveneur, S. Physicochemical Properties for the Reaction Systems: Levulinic Acid, Its Esters, and γ-Valerolactone. *J. Chem. Eng. Data* **2020**, *65*, 3008-3020. https://doi.org/10.1021/acs.jced.9b00965.

(43) Wang, Y.; Plazl, I.; Vernières-Hassimi, L.; Leveneur, S. From Calorimetry to Thermal Risk Assessment: γ-Valerolactone Production from the Hydrogenation of Alkyl Levulinates. *Process Saf. Environ. Prot.* **2020**, *144*, 32–41. https://doi.org/10.1016/j.psep.2020.07.017.

(44) Chang, C.; Xu, G.; Jiang, X. Production of Ethyl Levulinate by Direct Conversion of Wheat

Straw in Ethanol Media. *Bioresour. Technol.* **2012**, *121*, 93–99. https://doi.org/10.1016/j.biortech.2012.06.105.

(45) Appaturi, J. N.; Johan, M. R.; Ramalingam, R. J.; Al-Lohedan, H. A.; Vijaya, J. J. Efficient Synthesis of Butyl Levulinate from Furfuryl Alcohol over Ordered Mesoporous Ti-KIT-6 Catalysts for Green Chemistry Applications. *RSC Adv.* **2017**, *7*, 55206-55214. https://doi.org/10.1039/c7ra10289e.

(46) Liu, C.; Lu, X.; Yu, Z.; Xiong, J.; Bai, H.; Zhang, R. Production of Levulinic Acid from Cellulose and Cellulosic Biomass in Different Catalytic Systems. *Catalysts*. **2020**, *10*, 1006. https://doi.org/10.3390/catal10091006.

(47) Signoretto, M.; Taghavi, S.; Ghedini, E.; Menegazzo, F. Catalytic Production of Levulinic Acid (LA) from Actual Biomass. *Molecules* **2019**, *24* (15), 2760. https://doi.org/10.3390/molecules24152760.

(48) van Boekel, M. A. J. S. On the Pros and Cons of Bayesian Kinetic Modeling in Food Science. *Trends Food Sci. Technol.* **2020**, *99*, 181–193. https://doi.org/10.1016/j.tifs.2020.02.027.

(49) Stewart, W. E.; Caracotsios, M. *Computer-Aided Modeling of Reactive Systems*, First Edition.
Wiley-Interscience. A John Wiley & Sons, Inc. publication: New Jersey, 2008. https://doi.org/10.1002/9780470282038.

(50) Stewart, W. E.; Caracotsios, M. Athena Visual Studio www.athenavisual.com (accessed Jun 10, 2020).

(51) Kopyscinski, J.; Choi, J.; Hill, J. M. Comprehensive Kinetic Study for Pyridine

Hydrodenitrogenation on (Ni)WP/SiO2 Catalysts. *Appl. Catal. A Gen.* **2012**, *445–446*, 50–60. https://doi.org/10.1016/j.apcata.2012.08.027.

(52) Stewart, W. E.; Caracotsios, M.; Sørensen, J. P. Parameter Estimation from Multiresponse Data. *AIChE J.* **1992**, *38* (5), 641–650. https://doi.org/10.1002/aic.690380502.

(53) Hsu, S. H.; Stamatis, S. D.; Caruthers, J. M.; Delgass, W. N.; Venkatasubramanian, V.; Blau, G. E.; Lasinski, M.; Orcun, S. Bayesian Framework for Building Kinetic Models of Catalytic Systems. *Ind. Eng. Chem. Res.* **2009**, *48* (10), 4768–4790. https://doi.org/10.1021/ie801651y.

(54) Savara, A.; Walker, E. A. CheKiPEUQ Intro 1: Bayesian Parameter Estimation Considering Uncertainty or Error from Both Experiments and Theory. *ChemCatChem* **2020**, *12* (21), 5385–5400. https://doi.org/10.1002/cctc.202001566.

(55) Walker, E. A.; Ravisankar, K.; Savara, A. CheKiPEUQ Intro 2: Harnessing Uncertainties from Data Sets, Bayesian Design of Experiments in Chemical Kinetics. *ChemCatChem* **2020**, *12* (21), 5401–5410. https://doi.org/10.1002/cctc.202000976.

(56) Stewart, W. E.; Shon, Y.; Box, G. E. P. Discrimination and Goodness of Fit of Multiresponse Mechanistic Models. *AIChE J.* **1998**, *44* (6), 1404–1412. https://doi.org/10.1002/aic.690440618.

(57) Kopyscinski, J.; Schildhauer, T. J.; Vogel, F.; Biollaz, S. M. A.; Wokaun, A. Applying Spatially Resolved Concentration and Temperature Measurements in a Catalytic Plate Reactor for the Kinetic Study of CO Methanation. *J. Catal.* **2010**, *271* (2), 262–279. https://doi.org/10.1016/j.jcat.2010.02.008.

(58) Thakar, N.; Berger, R. J.; Kapteijn, F.; Moulijn, J. A. Modelling Kinetics and Deactivation for the Selective Hydrogenation of an Aromatic Ketone over Pd/SiO2. *Chem. Eng. Sci.* **2007**, *62* (18–20), 5322–5329. https://doi.org/10.1016/j.ces.2007.01.059.

(59) Bernacki, J. P.; Murphy, R. M. Model Discrimination and Mechanistic Interpretation of Kinetic Data in Protein Aggregation Studies. *Biophys. J.* **2009**, *96* (7), 2871–2887. https://doi.org/10.1016/j.bpj.2008.12.3903.

(60) Bressa, S. P.; Martínez, O. M.; Barreto, G. F. Kinetic Study of the Hydrogenation and Hydroisomerization of the N-Butenes on a Commercial Palladium/Alumina Catalyst. *Ind. Eng. Chem. Res.* **2003**, *42* (10), 2081–2092. https://doi.org/10.1021/ie0209879.

(61) Alves, J. A.; Bressa, S. P.; Martínez, O. M.; Barreto, G. F. Kinetic Study of the Selective Catalytic Hydrogenation of 1,3-Butadiene in a Mixture of n-Butenes. *J. Ind. Eng. Chem.* **2012**, *18* (4), 1353–1365. https://doi.org/10.1016/j.jiec.2012.01.038.

(62) Behravesh, E.; Melander, M. M.; Wärnå, J.; Salmi, T.; Honkala, K.; Murzin, D. Y. Oxidative Dehydrogenation of Ethanol on Gold: Combination of Kinetic Experiments and Computation Approach to Unravel the Reaction Mechanism. *J. Catal.* **2020**, *394,* 193-205. https://doi.org/10.1016/j.jcat.2020.07.022.

(63) Matera, S.; Schneider, W. F.; Heyden, A.; Savara, A. Progress in Accurate Chemical Kinetic Modeling, Simulations, and Parameter Estimation for Heterogeneous Catalysis. *ACS Catal.* **2019**, *9* (8), 6624–6647. https://doi.org/10.1021/acscatal.9b01234.

(64) McDonald, M. A.; Bromig, L.; Grover, M. A.; Rousseau, R. W.; Bommarius, A. S. Kinetic Model Discrimination of Penicillin G Acylase Thermal Deactivation by Non-Isothermal

Continuous Activity Assay. *Chem. Eng. Sci.* **2018**, *187*, 79–86. https://doi.org/10.1016/j.ces.2018.04.046.

TOC graphic

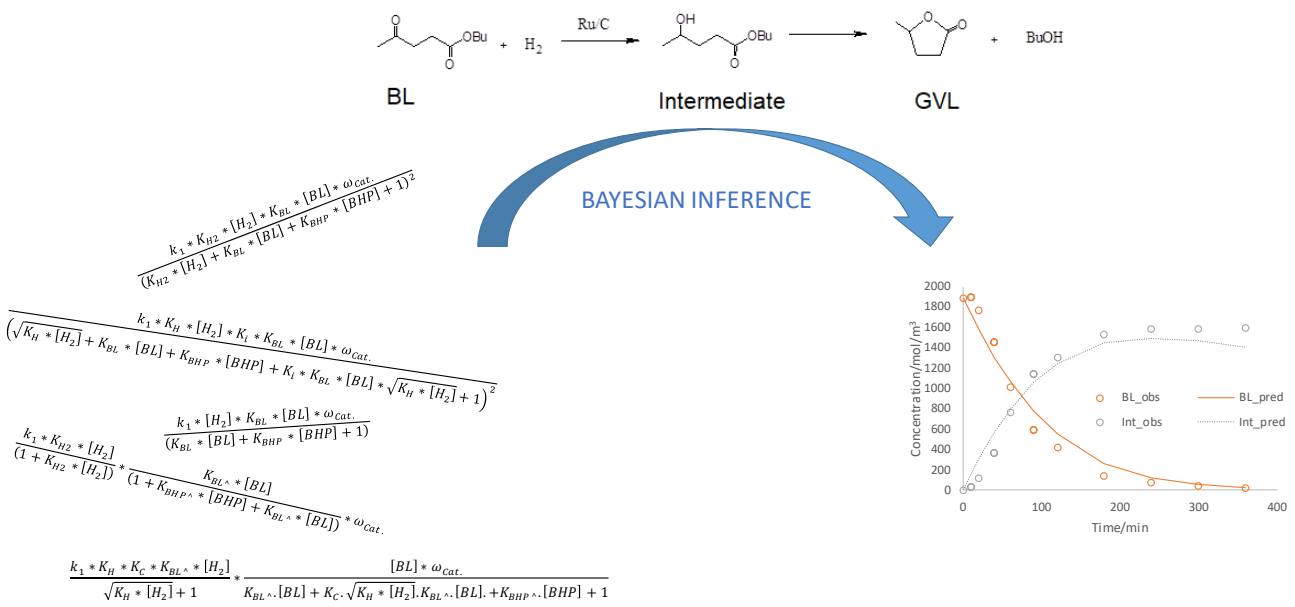

Which model?

Non-competitive Langmuir-Hinshelwood with no dissociation of hydrogen